PHYSICAL REVIEW B VOLUME 32, NUMBER 4 15 AUGUST 1985

Ab initio relativistic pseudopotential study of the zero-temperature structural properties of SnTe and PbTe

K. M. Rabe and J. D. Joannopoulos
Department of Physics, Massachusetts Institute of Technology, Cambridge, Massachusetts 02139

(Received 1 February 1985)

The equilibrium lattice parameters, bulk moduli, cohesive energies, $\mathbf{k}=0$ TO-phonon frequencies and elastic constant C_{44} of SnTe and PbTe are calculated completely from first principles with use of the local-density-functional pseudopotential total-energy method including relativistic effects. Good agreement with experiment is obtained. The approximation of neglecting spin-orbit coupling is found to be adequate for most purposes. Band structures and valence charge densities are presented. The latter are seen to differ significantly from previous empirical-pseudopotential-method calculations. The form of $\omega_{\mathrm{TO}}(P)$ in PbTe is found to be linear for small pressures P. Some possibilities for further applications of this method to these materials are discussed.

I. INTRODUCTION

Understanding of the physics of the IV-VI semiconducting compounds $A^{\mathrm{IV}}B^{\mathrm{VI}}(A^{\mathrm{IV}}=\mathrm{Ge}$, Sn, Pb; $B^{\mathrm{VI}}=\mathrm{S}$, Se, Te) has greatly improved over recent years. The initial focus was on the band structures of compounds with rocksalt structure: PbS, PbSe, PbTe, and at high temperature, SnTe and GeTe. These are semiconductors, with a narrow gap of several tenths of an eV at the L point. The band edges are highly nonparabolic, and the ordering of the levels at L is composition sensitive and determines the temperature and pressure coefficients of the band gap. These features, which are important for calculating transport properties, have been studied extensively both experimentally and with a variety of band-structure techniques including augmented plane wave (APW), orthogonalized plane wave (OPW), Korringa-Kohn-Rostoker (KKR), and empirical pseudopotential method (EPM).[1] The IV-VI compounds and pseudobinary alloys are observed to crystallize in orthorhombic, rhombohedral, and CsCl structures, as well as rocksalt, as a function of composition, pressure, and temperature. The tendency of the telluride compounds towards a transition from the rocksalt structure to a rhombohedral structure (Fig. 1) with decreasing temperature is of particular experimental[2] and theoretical[3] interest. In addition to being the simplest possible structural type of ferroelectric transition, with two atoms per unit cell in both the high-temperature and low-temperature structures, it is associated with an easily identifiable soft mode (the $\mathbf{k}=0$ TO phonon) and is second order. However, attempts at a fully quantitative understanding of this transition are hindered by experimental and theoretical difficulties inherent in the materials.

A variety of experimental techniques have been developed to study structural transitions and soft-mode behavior in ferroelectrics.[4] The application of these techniques to PbTe, SnTe, and GeTe is complicated by the free carriers arising from defects in the crystals. While the nature of various defects, especially in PbTe, is itself quite an active area of study,[1] for the purpose of this discussion the important defects are group-IV or Te vacancies. The electronic states associated with these vacancies lie deep in the bands so the free carriers do not freeze out at any temperature.[5] The crystal properties are very sensitive to the presence of the defects. In SnTe, variations in T_c from <0 to 100 K are well correlated with free-carrier concentration.[6,7]

The change in crystal structure with temperature has been studied directly in SnTe and GeTe using x-ray diffraction[8,9] and elastic neutron scattering.[10] The distorted structures are described by a rhombohedral Bravais lattice of angle α (equal to 60° in the fcc structure) and a basis with atoms at $a_0(0,0,0)$ and $a_0(0.5-\tau,0.5-\tau,0.5-\tau)$. Thus τ parametrizes the sublattice displacement, i.e., the amplitude of the frozen-in optic phonon as shown in Fig. 1. τ and α appear to be continuous at the transition temperature, indicating a second-order (or at most very weakly first-order) transition.

The temperature dependence of the soft-mode frequency has been measured using inelastic neutron scattering,[11–13] far-infrared spectroscopy in PbTe (Refs. 14 and 15) and, in the rhombohedral phase, Raman scattering.[6,16,17] The temperature dependence is observed to obey a Curie-Weiss law

$$\omega^2 \propto \begin{cases} T-T_c, & T>T_c \\ T_c-T, & T<T_c \end{cases}$$

with values $T_c>0$ for SnTe and GeTe and $T_c<0$ for PbTe. Thus in PbTe the tendency towards instability can be studied even though no actual transition takes place. Other relevant measurable quantities include an anomalous resistivity near the transition due to large thermal populations of the soft phonons,[18,19] and specific heat, which shows a mean-field-like jump near T_c.[20]

In the Cochran-Anderson soft-mode theory of ferroelectricity,[21,22] the stability of the lattice is studied by looking at its normal modes. In a lattice which exhibits a structural transition, some modes near the zone center are imaginary in the harmonic approximation. The strongly temperature-dependent renormalization of the phonon frequency by anharmonic terms stabilizes the lattice for

©1985 The American Physical Society

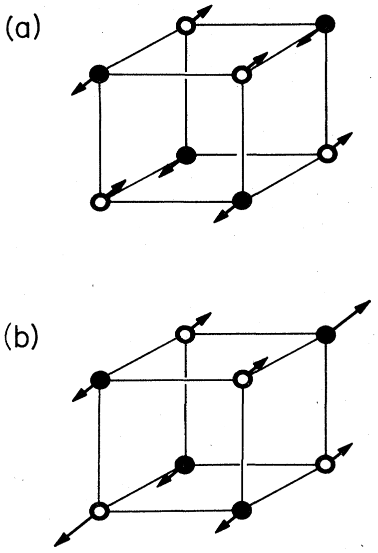

FIG. 1. Low-temperature rhombohedral structure of SnTe and GeTe can be obtained as a small distortion of the rocksalt structure by (a) displacing the two fcc sublattices relative to each other by $a_0\tau(111)$, corresponding to a frozen-in $\mathbf{k}=0$ optic phonon, followed by (b) a rhombohedral shear in the (111) direction which changes the rhombohedral angle from its fcc value of 60° to α.

$T > T_c$. Thus, within this theoretical framework the investigation naturally divides into two parts.

First, the mechanism which makes the symmetric structure unstable at zero temperature must be analyzed and a quantitative model developed which at least reproduces chemical trends. The large ϵ_0, Z^* and mixed ionic-covalent nature of the bonding in the tellurides suggest that resonant p-bonding results in a large electron-phonon coupling which drives the instability[23]. Several empirical pseudopotential models based on this idea have been developed.[24–26] One interesting result which emerges from the analysis of Littlewood[24] and Porod and Vogl[25] is that the lattice instability is not a consequence of the narrow band gap, but results from a combination of crystal geometry and the balance between ionicity and covalency.

Second, finite-temperature effects must be incorporated into the theory. This is done by finding a model Hamiltonian to describe the anharmonic processes which stabilize the structure at sufficiently high temperatures. In an anharmonic lattice model, a Hamiltonian which includes the coupling of the soft mode to the rest of the phonons is solved in quasiharmonic or self-consistent-phonon approximations.[27] A local-mode model formulates the problem in real space, using as degrees of freedom the amplitudes of atomic displacements corresponding to the soft mode within each unit cell and solving in mean-field theory.[28] These models reproduce qualitatively the temperature dependence of the soft mode, but have difficulties quantitatively.[29] A nonlinear shell model which includes the nonlinear quartic polarizability of the chalcogenide ion[30,31] succeeds, with relatively few empirical parameters, in quantitatively reproducing the temperature dependence of the soft mode as well as certain anomalies in the phonon dispersion relations.

All theoretical descriptions of the electronic and structural properties of the IV-VI materials have relied on empirical input. Experimentally it is known that the properties of the materials depend strongly on defect concentrations and extrapolation to a pure system is not well understood. Thus, empirically derived theoretical parameters implicitly contain defect effects, usually in some complex way.

In this paper we undertake the first *ab initio* theoretical investigation of the electronic and structural properties of SnTe and PbTe. We present results of relativistic pseudopotential total-energy calculations in the local-density approximation (LDA) for rocksalt structures and rhombohedral structures with various values of the parameters τ and α. A nonrelativistic approach has previously been applied to study bulk crystals, phonons, defects, and surfaces in metals,[32–34] semiconductors,[35–38] and insulators[39–42] with considerable quantitative success.[43] With the inclusion of relativistic effects to $O((e^2/\hbar c)^2)$ and the very high accuracy calculation possible because of the simplicity of the structure, we can expect similar success in SnTe and PbTe.

In Sec. II we discuss the application of the relativistic pseudopotential total-energy method to this system. In Secs. III and IV we present and discuss the results in the rocksalt structure for lattice constant, bulk modulus, cohesive energy, pseudocharge density, and band structures. In Sec. V we look at results in distorted structures for stability against distortion, pseudocharge density, and band structures. In Sec. VI we discuss the $\mathbf{k}=0$ TO phonon in PbTe. Finally, in Sec. VII we summarize our results and make some concluding remarks.

II. METHOD

The theory and practice of self-consistent pseudopotential total-energy calculations have been thoroughly discussed elsewhere.[44,45] The total energy can be written in the following form:

$$E_{\text{tot}} = E_{\text{kin}} + E'_{ei} + E'_H + E_{\text{xc}} + E'_{ii} \ , \tag{1}$$

where E_{kin} is the total kinetic energy of the electrons; E'_{ei} is the electron-ion interaction energy; E'_H is the Hartree energy; E_{xc} is the exchange correlation energy; and E'_{ii} is the ion-ion interaction energy. This expression is evaluated in the momentum space formalism.[46] The primes indicate that the separately divergent $q=0$ contributions are excluded. We use the relativistic nonlocal atomic pseudopotentials for Sn, Pb, and Te given by Bachelet, Hamann, and Schlüter[47] (BHS) shown in Fig. 2. Exchange and correlation are included through the LDA using the Ceperley-Alder-Perdew-Zunger (CAPZ) parametrization.[48] Eigenfunctions are expanded in the plane-wave basis $\{ |\mathbf{k}+\mathbf{G}\rangle : (\mathbf{k}+\mathbf{G})^2 < E_1 \}$. The effect of plane waves with $E_1 < (\mathbf{k}+\mathbf{G})^2 < E_2$ is included using Lowdin perturbation theory.[49] Brillouin-zone averages are performed using the special—$\mathbf{k}$-point scheme of Monkhorst and Pack.[50] E'_{ii} is obtained using the method described in Ref. 35. Computations were done on an IBM 370/3033 computer in single precision for Secs. III and IV and in

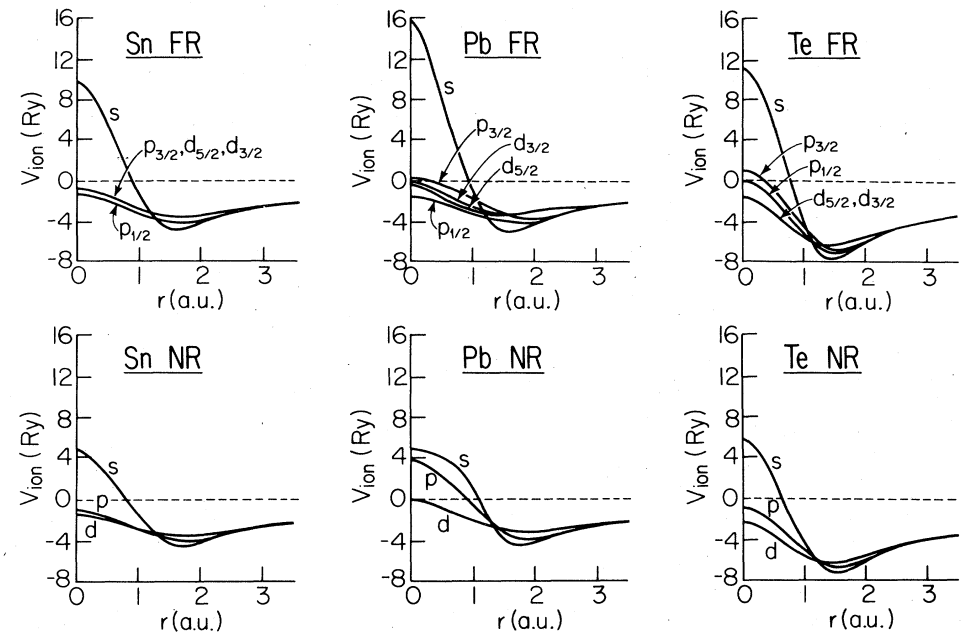

FIG. 2. Nonlocal ionic pseudopotentials for Sn, Pb, and Te. In the top row are shown the fully relativistic potentials constructed by BHS (Ref. 47) which are nonlocal in j and l, requiring five different potentials $s_{1/2}$, $p_{1/2}$, $p_{3/2}$, $d_{3/2}$, $d_{5/2}$. Scalar relativistic s, p, d potentials are obtained from the weighted average $\hat{V}_l=[1/(2l+1)][l\hat{V}_{l-1/2}+(l+1)\hat{V}_{l+1/2}]$ and are not shown here. In the bottom row are shown the nonrelativistic pseudopotentials constructed according to Ref. 55, with detailed information given in Table I. In all crystal calculations, the p potential is used as the local potential.

double precision for Secs. V and VI.

The method used by BHS to construct atomic pseudopotentials which contain all relativistic effects to $O((e^2/\hbar c)^2)$ was first introduced by Kleinman.[51,52] The point is that although all-electron calculations in a heavy atom must be done using the Dirac equation, the valence electron wave functions outside the core region can be well described by retaining only the major component of the Dirac wave function. The radial wave function obeys an effective Schrodinger equation outside the core. By performing a normconserving pseudization on the all-electron Dirac atom, pseudopotentials V_{lj} are obtained, where the nodeless solution of the Schrodinger equation specified by a given V_{lj} matches the corresponding major component of the Dirac wave function outside the core region. Errors of $O((e^2/\hbar c)^2)$ occur in the decoupling of the major and minor components and in the neglect of the contribution of the minor component to the charge density outside the core.

The use of these pseudopotentials in crystal calculations involves only a straightforward modification of the nonrelativistic scheme

$$\hat{V}=\sum_l |l\rangle V_l\langle l| \rightarrow \sum_{l,j} |lj\rangle V_{lj}\langle lj| \ , \qquad (2)$$

so that the number of nonlocal potentials increases and the size of the plane-wave basis must be doubled ($|\mathbf{k}\rangle \rightarrow |\mathbf{k}\uparrow\rangle, |\mathbf{k}\downarrow\rangle$). In practice, these changes require a substantial increase in computational effort, both in the setup of the Hamiltonian matrix and in diagonalization. However, all relativistic effects except spin-orbit splitting can be included by writing

$$\hat{V}=\sum_l |l\rangle (V^l_{\text{ion}}+V^l_{\text{s.o.}}\mathbf{L}\cdot\mathbf{S})\langle l| \qquad (3)$$

and neglecting $V^l_{\text{s.o.}}$, which restores the problem to its nonrelativistic size. For a semiconductor, inclusion of $\hat{V}_{\text{s.o.}}$ in first-order perturbation theory does not change the charge density, and if higher-order corrections are unimportant the total energy is approximately unaffected. These scalar relativistic (SR) potentials are used for all calculations unless otherwise specified. We examine the effects of this approximation by comparing fully relativistic (FR) and SR results for some test cases. We also compare SR calculations to results in PbTe and SnTe obtained using atomic pseudopotentials (Fig. 2) constructed using nonrelativistic (NR) atomic calculations and the parameters of Table I.

The accuracy of the computation of pseudocrystal total energy is mainly limited by (i) the representation of the wave functions in terms of a finite basis set and (ii) the approximation of Brillouin-zone averages using a finite sample of $\mathbf{k}$ points. The smallness of the unit cell makes a high level of convergence possible using available computation facilities (IBM 370/3033). Convergence is evaluated by looking at changes in energy differences between different structures, rather than at the absolute value of energy. For the calculations in the RS structure, good convergence in lattice constant and bulk modulus (typical errors in energy differences $\sim 10^{-4}$ Ry) was achieved with $E_1=10.5$, $E_2=16.5$ Ry (~ 250 plane

TABLE I. Construction of nonrelativistic pseudopotentials for Sn, Pb, and Te. *s*, *p*, and *d* potentials are calculated from a single atomic configuration. r_c is the core radius parameter described in Ref. 55, adjusted to optimize the smoothness and shallowness of the potentials. The energy eigenvalues of the nonrelativistic pseudoatoms are compared with those of the BHS FR pseudoatoms given in parentheses.

		Eigenvalues (in Ry)			r_c (in a.u.)		
	Configuration	*s*	*p*	*d*	*s*	*p*	*d*
Sn	$s^1p^{0.75}d^{0.25}$	-1.96276	-1.40928	-0.71013	1.41	1.57	1.80
		(-2.05024)	$(-1.46054, -1.40408)$	$(-0.70427, -0.69930)$			
Pb	$s^1p^{0.75}d^{0.25}$	-1.88196	-1.35142	-0.68616	1.25	1.40	1.80
		(-2.16814)	$(-1.52106, -1.34200)$	$(-0.67282, -0.65820)$			
Te	$s^1p^{2.75}d^{0.25}$	-2.40357	-1.72558	-0.83167	1.28	1.35	1.50
		(-2.52152)	$(-1.79768, -1.71331)$	$(-0.82143, -0.81388)$			

waves in basis set), and 10 **k** points (single precision). Calculations in distorted structures required better energy resolution [$\sim(2-3)\times10^{-5}$ Ry] and so larger **k**-point sets (usually 32 **k** points but up to 60) were necessary. The results of total-energy calculations are generally insensitive to the precise form of the local-density functional,[45] but we could not test this because only relativistic atomic potentials calculated with CAPZ were available.

A calculation of the total energy of the free pseudoatoms is required to determine the cohesive energy. The observed term values for the atomic ground state are $^3P_0$ for Sn and Pb and $^3P_2$ for Te. The total energies of the scalar relativistic pseudoatoms are calculated, a spin-polarization correction is made and the spin-orbit energy lowering is obtained in first-order perturbation theory in $\hat{V}_{\text{s.o.}}$. We neglect the mixing of terms by the spin-orbit interaction, although in Pb the spin-orbit perturbation (0.892 eV) is even larger than the energy lowering from the spin polarization (0.669 eV), and in Sn and Te the spin-orbit correction is only about a factor of 3 smaller than the spin-polarization correction.

III. ROCKSALT STRUCTURE

SnTe above its transition temperature and PbTe are observed to crystallize in the rocksalt structure, which can be described as an fcc Bravais lattice of conventional side a_0 with a basis of a Pb or Sn atom at $a_0(0,0,0)$ and a Te atom at $a_0(0.5,0.5,0.5)$. A given rocksalt structure is specified completely by a single parameter—the volume per atom $V=a_0^3/8$. To obtain the equilibrium lattice constants, bulk moduli and cohesive energies of SnTe and PbTe in the RS structure, total energies per atom are calculated at several values of V near V_{expt} and fitted to a cubic polynomial. Calculated points deviate from the fitted curve by $<10^{-4}$ Ry/atom. The results for NR and SR SnTe are shown graphically in Fig. 3. The minimum of the NR curve occurs at a lower value of V than that of the SR curve, and has noticeably higher curvature at the minimum, corresponding to a larger bulk modulus. The NR curve is shifted upwards in energy from the SR curve by about 0.2 Ry/atom. In Fig. 4, the various terms contributing to the total energy of SR SnTe are plotted as a function of V. As the structure is expanded, E_{kin} de-

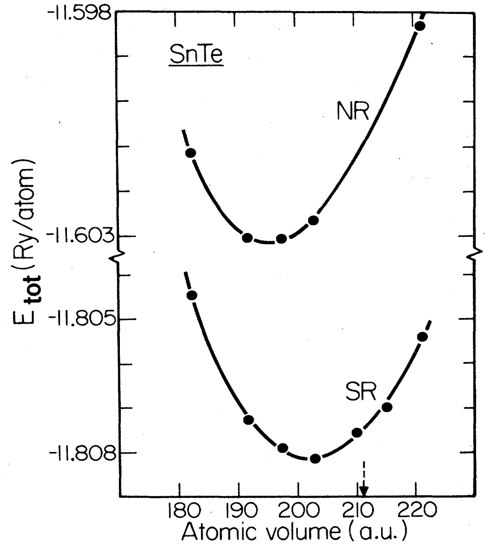

FIG. 3. Total energy (in Ry) in the rocksalt structure as a function of volume per atom [in $(Br)^3$] for SnTe. Each vertical tick equals 10^{-3} Ry. The upper data points are calculated using the NR potentials. The lower points are obtained using the SR potentials. Cubic polynomial fits are shown as solid lines.

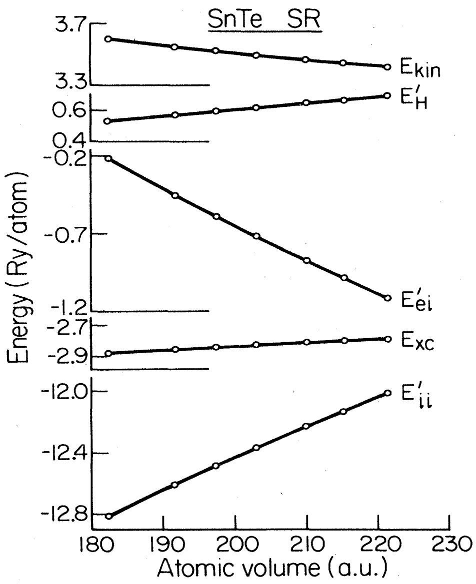

FIG. 4. Contributions to the SR total energy of SnTe in the rocksalt structure as described in the text. Each vertical tick equals 0.1 Ry.

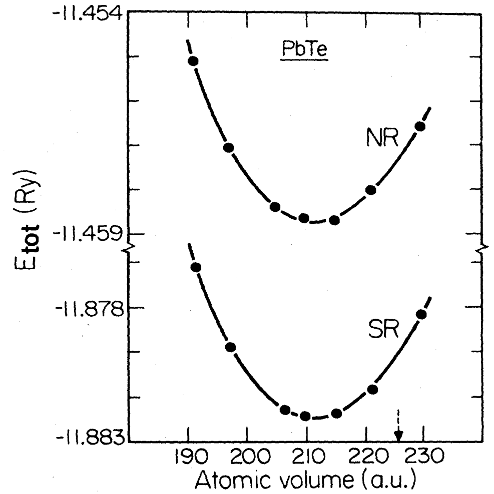

FIG. 5. Total energy in the rocksalt structure as a function of atomic volume for PbTe. Same convention as in Fig. 3.

creases slightly, while E_{xc} and E'_H show a small increase. The dominant changes are the increase in the Ewald energy E'_{ii}, which depends only on the lattice structure and ionic charges and favors low atomic values and high coordination number, and the electron-ion interaction energy E'_{ei}, which decreases as charge moves from the interatomic regions to become more localized around individual ions.

The E_{tot} (V) results for NR and SR PbTe are shown in Fig. 5. Here, the minima and curvatures of the NR and SR curves are very similar; however, the overall shift of the NR energies up from the SR energies is about 0.4 Ry/atom, twice as large as the shift in SnTe. The contributions to $E_{tot}(V)$ of SR PbTe are plotted in Fig. 6. The same trends are evident as in SR SnTe, though there are quantitative differences responsible for the different V_0 and B.

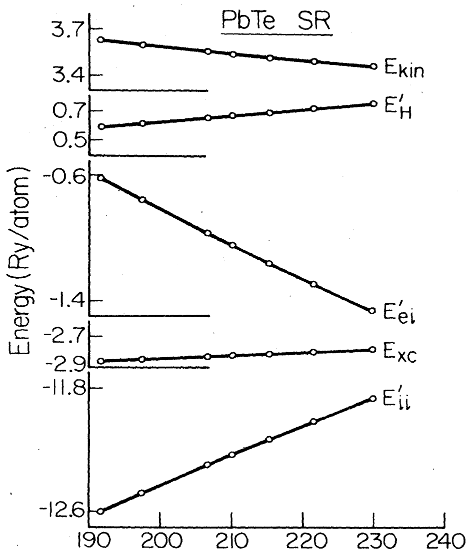

FIG. 6. Contributions to the SR total energy of PbTe in the rocksalt structure. Same convention as in Fig. 4.

TABLE II. Structural properties of SnTe and PbTe calculated using nonrelativistic (NR), scalar relativistic (SR), and fully relativistic (FR) atomic pseudopotentials, compared to experimental values.

	Crystal energy in Ry/atom	Cohesive energy (eV)	Lattice constant (Å)	Bulk modulus (Mbar)
SnTe				
NR	−11.60314	7.5	6.14	0.59
SR	−11.80814	7.2	6.21	0.49
FR	−11.81250	6.9	6.23	0.51
Expt.		5.7[a]	6.295 (0 K)[b] 6.327 (300 K)[d]	0.378,0.278 (300 K)[c] 0.46 (0 K)[e] 0.42 (300 K)[f] 0.47 (4.2 K)[g]
PbTe				
NR	-11.45875	7.5	6.31	0.48
SR	-11.88251	7.2	6.31	0.48
FR	-11.89644	6.4	6.29	0.45
Expt.		4.7[a]	6.443 (300 K)[h] 6.462 (300 K)[j]	0.456±0.004(0 K)[i]

[a] Cohesive energy is obtained from cohesive energies of the elements[56] and heats of formation of the compounds.[57]

[b] Reference 8.

[c] Reference 59.

[d] Reference 58.

[e] Reference 60.

[f] Reference 61.

[g] Reference 62.

[h] Reference 63.

[i] Reference 54.

[j] Reference 64.

The physical parameters extracted from the fits are given in Table II for comparison with the corresponding experimental values. PbTe is observed to remain rocksalt down to the lowest temperatures at which measurements have been made, with a value of $T_c \approx -100$ K extrapolated from the Curie-Weiss temperature dependence of the $\mathbf{k}=0$ TO phonon. The calculated SR lattice constant agrees with the observed room-temperature value to within 2% and the calculated and observed bulk moduli agree to 5%. For SnTe, the comparison with experiment is less definitive than for PbTe, since pure samples do not crystallize in the rocksalt structure at low temperature. Thus we compare results calculated in the rocksalt structure with data taken at 300 K or at low temperature in samples in which the transition temperature is suppressed by the defect concentration. The calculated SR lattice constant agrees with the experimental value to $\sim 1\%$. The SR calculated bulk modulus is higher than any of the available experimental values but the variation in these is so large that the value of a more quantitative comparison is doubtful. We also include in the table results of FR calculations which help to support our claim in Sec. II that a scalar relativistic description is adequate for the calculation of total-energy differences between different structures.

The calculated FR cohesive energy is off from experiment by 36% for PbTe and 20% for SnTe. Neglecting the spin-orbit interaction entirely gives nearly equal cohesive energies for SnTe and PbTe, while the experimental value for PbTe is 1 eV/pair lower than for SnTe. Thus, part of the error can be attributed to the treatment of the spin-orbit interaction in the atomic calculations. Errors due to the use of the local-density functional are also expected to be significant.

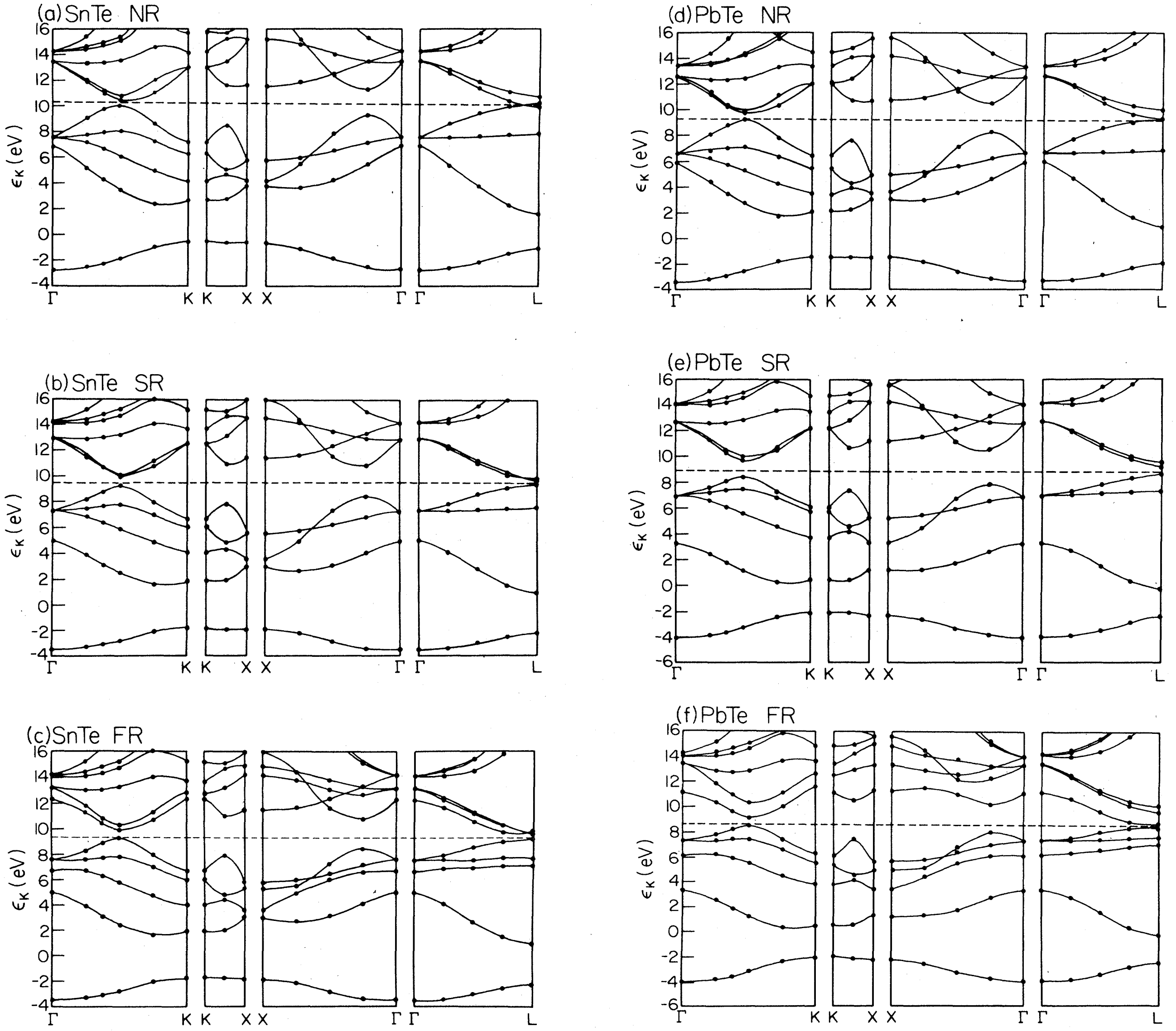

FIG. 7. Pseudopotential band structures in the rocksalt structure of (a)—(c) SnTe and (d)—(f) PbTe. For each material, three calculations are shown: NR, SR, and FR, respectively.

IV. ROCKSALT BAND STRUCTURES AND CHARGE DENSITIES

In Fig. 7 we present the band structures of SnTe and PbTe calculated at V_0 for NR, SR, and FR potentials. The general features compare favorably with previous calculations. Since we are primarily interested in calculating total energies, which involves averaging valence-band properties over the Brillouin zone, we have not studied in detail features of the band structure such as level ordering and gap structure in the immediate neighborhood of L. A comparison of the SR and FR band structures shows that while the spin-orbit interaction certainly has a significant effect on the band structure, it mainly acts to lift the degeneracies within groups of scalar relativistic levels. The spin-orbit splitting of the upper valence band at point Γ increases only 30%, from 0.88 to 1.2 eV, in going from SnTe to PbTe, suggesting these levels have mostly Te p character, where Te has an atomic spin-orbit splitting of 1.2 eV. The direct gap at point L is 0.4 eV in both FR SnTe and FR PbTe.

A comparison of SR and NR band structures shows some differences in the level orderings, especially near L. In fact, NR SnTe is not even a semiconductor, but rather a semimetal. Another important effect is the relativistic enhancement of the s-p splitting due to the Darwin term, which is clearly manifested in the atomic eigenvalues. In the crystal, the splitting between the two lowest bands, which are s-like, and the next three, which are p-like, is significantly larger in the SR case than in NR. The lowering in energy of the s levels is responsible for the large shift in E_{tot} for NR versus SR potentials observed above. However, as we have seen, this increased splitting does not have a significant effect on the calculated equilibrium properties since only the p levels are significant in bonding.

Total valence charge densities in the (100) plane for PbTe and SnTe are shown in Fig. 8. The results for PbTe can be directly compared with the EPM charge densities of Ref. 53. In the EPM calculation, the charge density smoothly increases from the interstitial region to reach its maximum at the atomic origin, with roughly the same peak value on the Pb atom as on the Te. In the current calculation, because of the repulsive nature of the pseudopotential, the charge density is zero at the atomic origins, increasing to a maximum on a shell around the atom, and then decreasing into the interstitial regions. The shell around the Pb atom is broad and is at nearly half the nearest-neighbor distance, while the shell around the Te is much more sharply peaked and more tightly bound. The position of the peak in the charge density outside the core is consistent with the expected behavior of 5s and 6s electrons.

Next we examine the charge density of PbTe band by band (Fig. 9). The band-by-band breakdown in SnTe is very similar and will not be shown. Band 1 is almost pure Te s, with the charge density reaching its maximum on a shell at about one-quarter the nearest-neighbor distance. Band 2 is mostly Pb s, with some Te p. This Pb charge shell represents the more tightly bound portion of the total charge associated with the Pb, though it still has a larger radius than the Te s shell. Band 3 and 4 are predominantly Te p as indicated by the lack of spherical symmetry in the charge distributions around the Te atoms. The charge around the Te atom in band 5 appears nearly spherically symmetric, but guided by the band structures, the angular decomposition of the wave functions in Ref. 53 and the occurrence of the peak at the radius of the other p bands rather than the s band, we conclude it to be also mainly Te p. Band 6, the lowest conduction band, is Pb p and Te s.

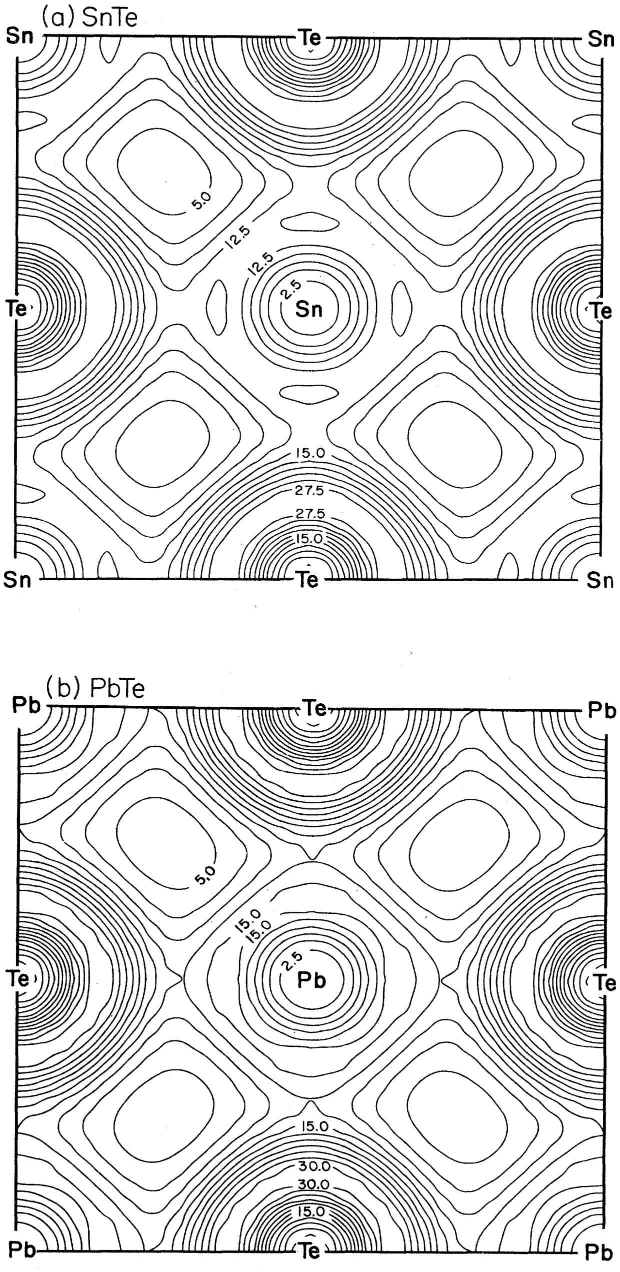

FIG. 8. Total valence pseudocharge densities plotted in the (100) plane of the rocksalt structure for (a) SnTe and (b) PbTe, in units of electrons per unit cell.

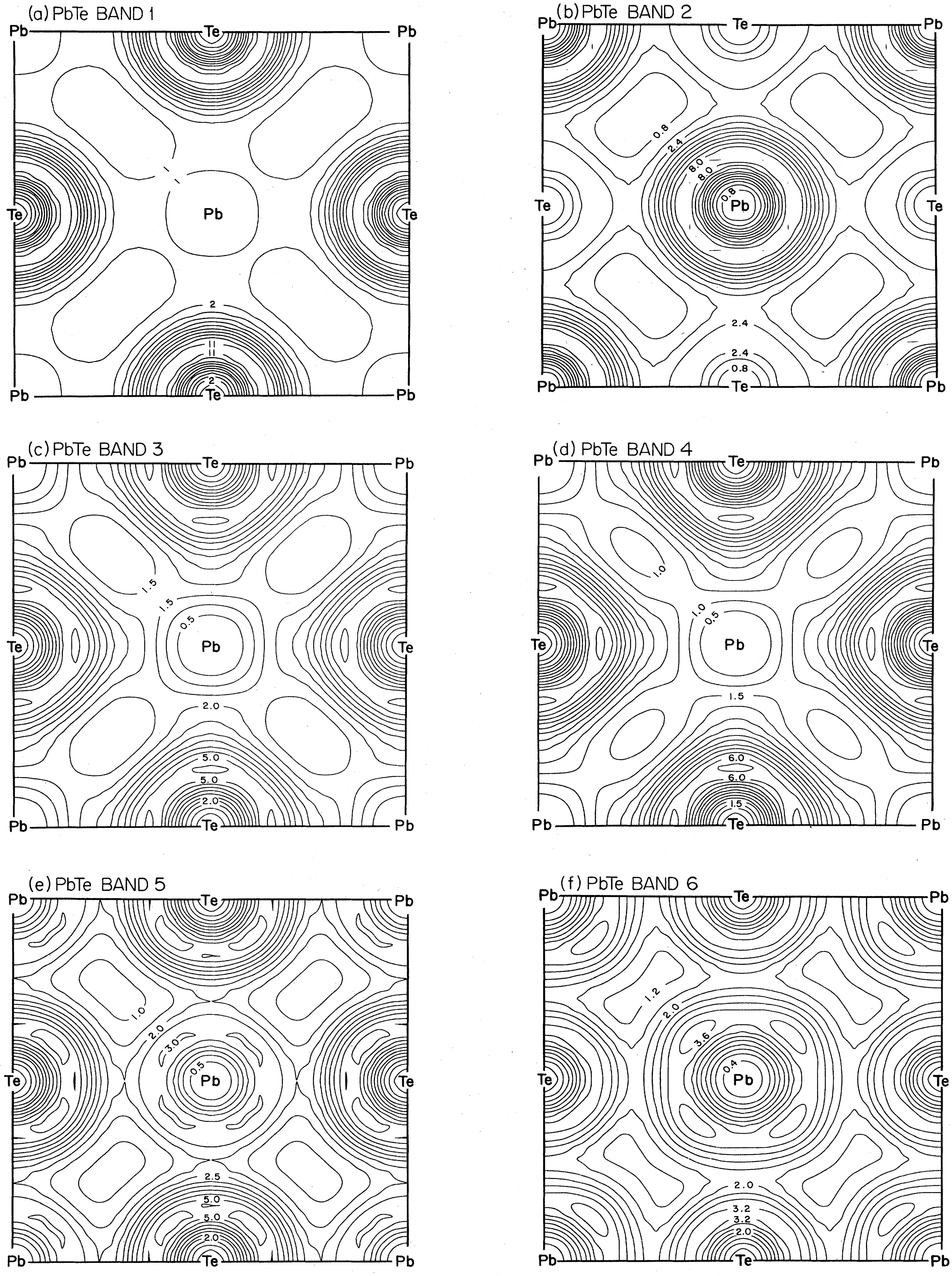

FIG. 9. Band-by-band pseudocharge densities plotted in the (100) plane of the rocksalt structure of PbTe for (a)—(e) bands 1—6, respectively, in units of electrons per unit cell.

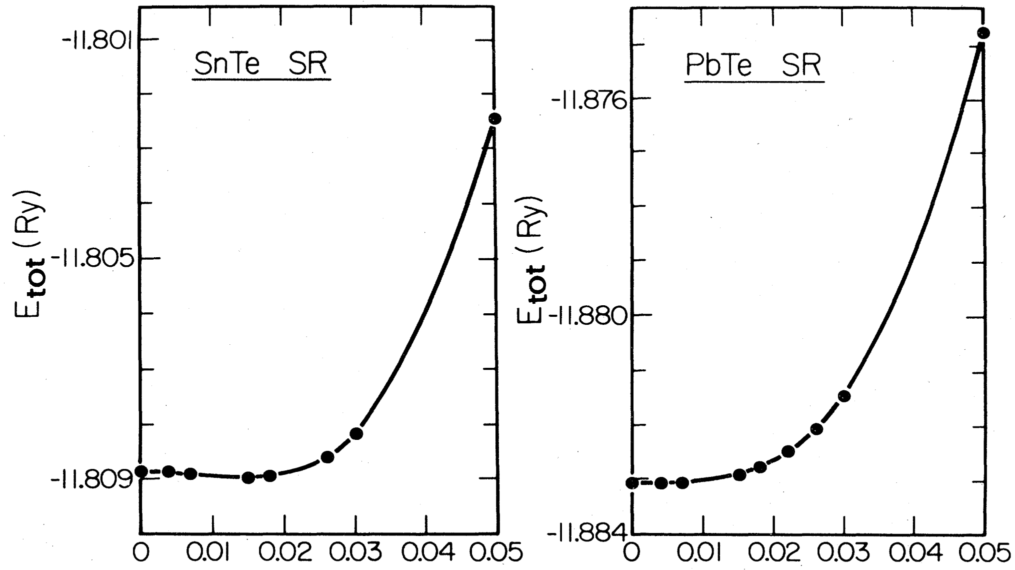

FIG. 10. Total energy in Ry of SnTe [$V=203.0(Br)^3$] and PbTe [$V=210.0(Br)^3$] as a function of τ with α fixed at 60°. Each vertical tick equals 10^{-3} Ry. Fits to polynomials cubic in τ^2 are shown as solid lines.

V. RHOMBOHEDRAL STRUCTURE

In this section we discuss results of total-energy calculations in the rhombohedral structure which can be obtained by a small distortion of the rocksalt structure (see Fig. 1). The rhombohedral Bravais lattice with symmetry axis along (111) is characterized by V and α, the angle between the primitive vectors (equal to 60° in the fcc structure). The basis consists of a Pb or Sn atom at $a_0(0,0,0)$ and a Te atom at $a_0(0.5-\tau, 0.5-\tau, 0.5-\tau)$. The three-dimensional structural parameter space is too large to be explored completely. A reasonable simplification is to fix V at the equilibrium volume obtained in the rocksalt calculations, which reduces the parameter space to $D=2$, making calculations feasible.

In Fig. 10 we investigate the stability of the rocksalt structure against the τ distortion only, holding α fixed at 60°. It is important to note that while the energy lowering driving the instability in SnTe appears small (1.1×10^{-4} Ry), it is quite definite and moreover is expected to be small, considering that $T_c \sim 100$ K. PbTe is stable against this distortion, though the phonon is soft. The plots of the contributions to $E_{\rm tot}(\tau)$ in SnTe and PbTe are very similar (Fig. 11). The Ewald energy E'_{ii} and the electronic

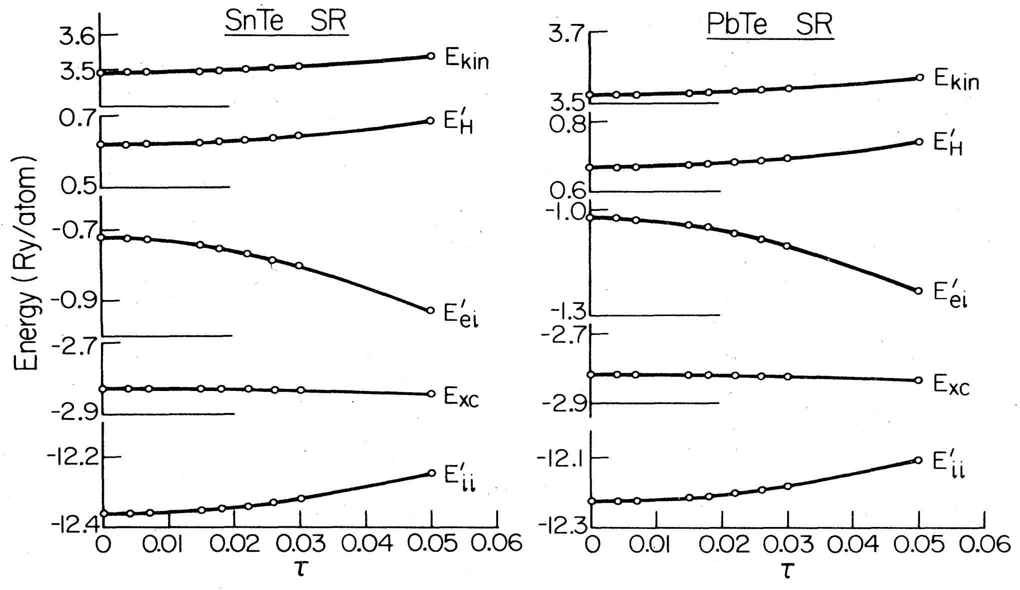

FIG. 11. Contributions to the total energy at $\alpha=60°$ as a function of τ for SnTe and PbTe. Same convention as in Fig. 4.

TABLE III. Contributions to total energy for undistorted and τ-distorted structures in SnTe and PbTe.

	SnTe $\left[\begin{array}{l}E_1=10.5\\ 19\ \mathbf{k}\ \text{points}\end{array}\right]$		PbTe $\left[\begin{array}{l}E_1=10.5\\ 32\ \mathbf{k}\ \text{points}\end{array}\right]$	
	$\tau=0.000$	$\tau=0.015$	$\tau=0.000$	$\tau=0.015$
E_{kin}	3.49239	3.49722	3.52250	3.52709
E_{xc}	−2.82877	−2.83086	−2.81985	−2.82175
E'_H	0.61630	0.62315	0.66629	0.67316
E'_{ei}	−2.79686	−2.81804	−3.10296	−3.12363
E'_{ii}	−12.36657	−12.35509	−12.22762	−12.21627
E_{tot}	−11.80887	−11.80898	−11.88329	−11.88305

energies E_{kin} and E'_H favor the more symmetric structure, while the electron-ion energy E'_{ei} acts to drive the instability. These trends are consistent with the resonant p-bonding picture. The qualitative difference in the $E_{\text{tot}}(\tau)$ curves for SnTe and PbTe is the result of a subtle quantitative change in these competing contributions. The values of the contributions at $\tau=0.000$ and $\tau=0.015$ for SnTe and PbTe are given in Table III.

In order to investigate the full two-dimensional parameter space, we extended our calculations to a mesh of (α,τ) values, plotting out $E_{\text{tot}}(\alpha,\tau)$ surfaces for PbTe and SnTe which are shown in Fig. 12. The τ distortion in SnTe is further stabilized by a change in α. The fit minimum is $\tau=0.015$ and $\alpha=59.5°$, which is in very reasonable agreement with the observed values $\tau=0.008$ and $\alpha=59.878°$ given that the relevant energy differences are an order of magnitude smaller than those required for the calculation of the lattice constant and bulk modulus. The results for PbTe are consistent with stability of the rocksalt structure. In particular, distortions in τ are energetically unfavorable at all values of α near 60°, while an estimate for the shear elastic constant C_{44} from the relation

$$\Delta E_{\text{tot}}(\Delta\alpha=\alpha-\pi/3,\ \tau=0)=\tfrac{3}{8}VC_{44}(\Delta\alpha)^2 \tag{4}$$

yields a value of 5×10^{11} dyn/cm^2, consistent with the observed value of 1.5×10^{11} dyn/cm^2.[54] Close examination of the behavior in PbTe of $E_{\text{tot}}(\alpha,\tau=0.000)$ for α near 60° shows that the global minimum occurs right at $\alpha=60°$, making the rocksalt structure an extremum as it must be by symmetry. Also, there is some indication of a local minimum about 10^{-4} Ry higher at $\alpha=60.4°$, though good resolution of this feature is beyond the accuracy of the current calculation.

Our success in obtaining the correct chemical trend of the instability is supported by calculations of total energies of rhombohedrally distorted GeTe, which show the same kind of instabilities as in SnTe with an energy gain about an order of magnitude larger, which is reasonable since the observed T_c in GeTe is 670 K compared to 100 K in SnTe. Study of the changes in charge density of SnTe with distortion in τ (Fig. 13) shows a movement of charge into the shorter bond and a deformation of the charge associated with the Te ion. The FR band structure for rhombohedral SnTe is shown in Fig. 14. The new features resulting from the distortion are the splitting of the bands into spin-polarized levels through the breaking of inversion symmetry arising from the τ distortion, and the division of the eight L points into the two inequivalent sets $\{(111),(\bar{1}\,\bar{1}\,\bar{1})\}$ and

$$\{(\bar{1}11),(1\bar{1}1),(11\bar{1}),(1\,\bar{1}\,\bar{1}),(\bar{1}1\bar{1}),(\bar{1}\,\bar{1}\,1)\}$$

by the rhombohedral distortion in the (111) direction. We

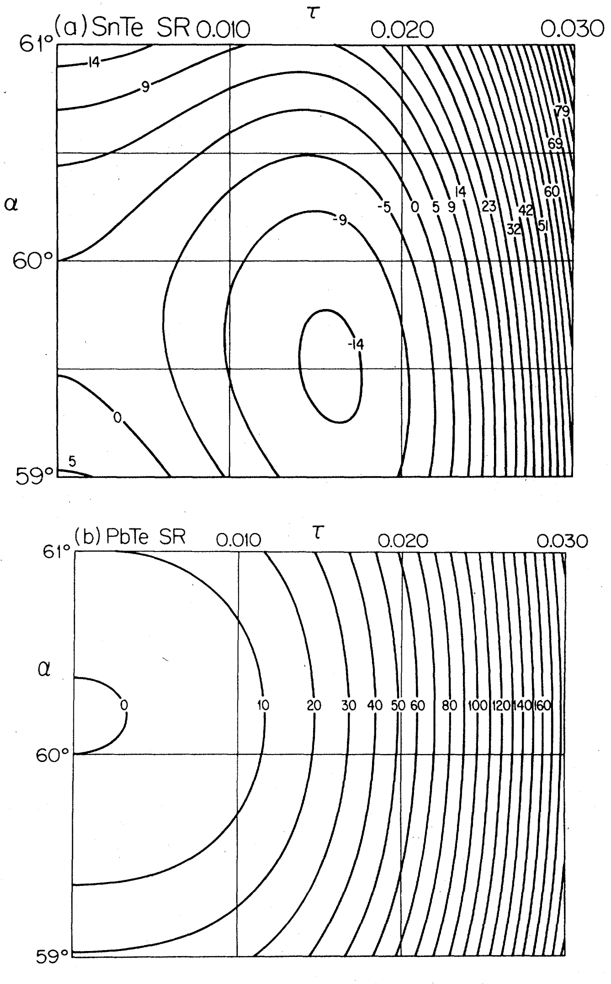

FIG. 12. Contour plot of the fit $\Delta E_{\text{tot}}(\alpha,\tau)=E_{\text{tot}}(\alpha,\tau)-E_{\text{tot}}(\alpha=60°,\ \tau=0.000)$ for (a) SnTe and (b) PbTe. Energies shown are in units of 10^{-5} Ry.

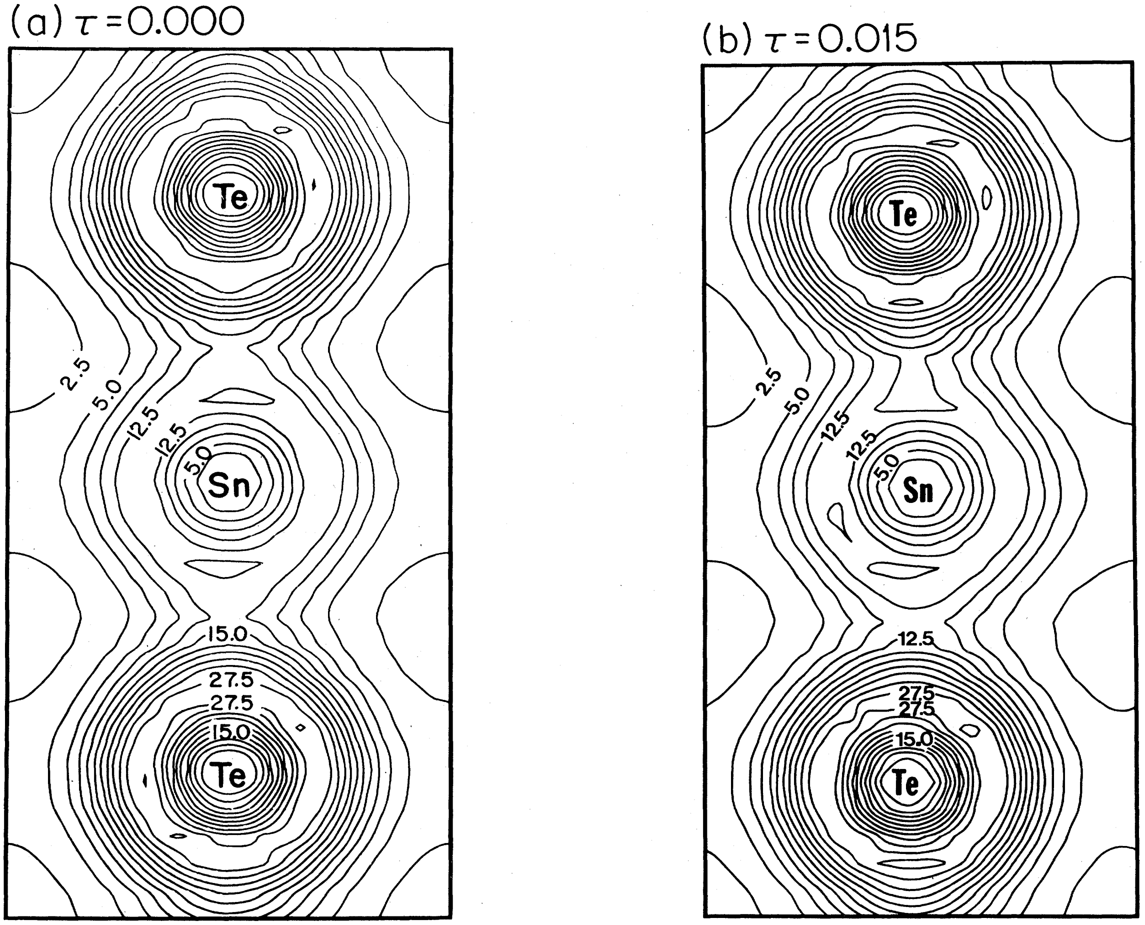

FIG. 13. Total valence pseudocharge densities in (110) plane of SnTe for (a) $\tau=0.000$ and (b) $\tau=0.015$. This section is advantageous since it slices through the bonds like the (100) section *and* the atoms stay in the plane for $\tau\neq0.000$. Charge densities are given in units of electrons per unit cell.

have not made a comparison of NR and SR potentials in the rhombohedral structure, but it would probably show a stabilization of the rocksalt structure through the relativistic s-p splitting enhancement, which makes s-p hydridization unfavorable. Tests show that the inclusion of spin-orbit splitting preserves the qualitative features of this discussion.

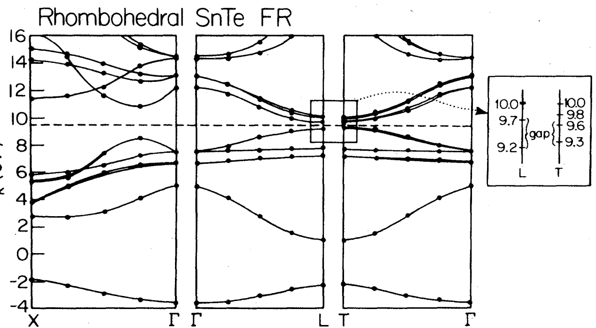

FIG. 14. Pseudopotential band structure of SnTe with $\alpha=59.5°$ and $\tau=0.015$ using fully relativistic potentials. The levels near the gap at the L and T points are compared in the detail.

VI. TO PHONON IN PbTe

In PbTe, although the calculation shows the rocksalt structure is stable, the $\mathbf{k}=0$ TO phonon is unusually soft. Its frequency can be obtained from a frozen phonon calculation, which is particularly simple in this case since the atomic displacement vectors are already known and the effective potential depends on the single parameter τ. The quadratic part of $V_{\text{eff}}(\tau)$ yields a harmonic approximation to the phonon frequency, but V_{eff} is quite anharmonic, and thus to compare to experiment we need the renormalized phonon frequency. In the self-consistent phonon approximation, with a polynomial fit

$$V_{\text{eff}}(\tau)=b_0+3a_0^2b_1\tau^2+9a_0^4b_2\tau^4+27a_0^6b_3\tau^6\ , \tag{5}$$

$\bar{\varpi}$ obeys

$$\tfrac{1}{2}M\bar{\omega}^2=b_1+\frac{3b_2\hbar}{M\bar{\omega}}\coth\left[\frac{\hbar\bar{\omega}\beta}{2}\right]+\frac{45}{2}\frac{b_3\hbar^2}{(M\bar{\omega})^2}\left[\frac{3}{2}+\frac{1}{4}\left[\frac{1}{\sinh^2(\hbar\bar{\omega}\beta/2)}+\coth^2(\hbar\bar{\omega}\beta/2)\right]\right], \tag{6}$$

where M is the reduced mass of the ions. We use this equation with $T=0$ and include only a constant coupling to a single optical branch. Very large **k** point sets (44 **k** points) are required to obtain convergence of ω_{TO}. Our SR values for the bare and renormalized phonon frequencies are 31 and 35 cm^{-1}, respectively, to be compared with the experimental value of 26 cm^{-1}.[15] The theoretical values are in reasonable agreement with experiment given that the frequencies are so low, i.e., that the relevant energy differences are so small. Among the effects we have left out are defects, which according to current models should raise the phonon frequency from its value in the perfect crystal.[2] Also, FR calculations with 19 **k** points indicate that the inclusion of spin-orbit splitting tends to lower the frequency.

In a recent experiment,[15] the Gruneisen parameters was measured to be about twice as large (19.6) as predicted values of dT_c/dP would imply. We have determined a value for the mode Gruneisen parameter

$$\gamma=\frac{B}{\omega_{\mathrm{TO}}}\frac{d\omega_{\mathrm{TO}}}{dP}$$

from calculations of the TO phonon frequency at four different values of V (Fig. 15). The rocksalt $E_{\mathrm{tot}}(V)$ calculations are used to determine $V(P)$ and B, the bulk modulus. The result is a Gruneisen parameter of about 7. Since the result is quite sensitive to the quantitative accuracy of the several quantities in the expression, this should be regarded as a very rough estimate and should not be used to determine definitely whether or not the observed large Gruneisen parameter is an intrinsic property of the material.

On the other hand, what these calculations definitely show is that $\omega_{\mathrm{TO}}(P)$ is very close to linear. This is important because it would rule out explanations for the large Gruneisen parameter which require a strong nonlinearity of $\omega_{\mathrm{TO}}(P)$ at small P.

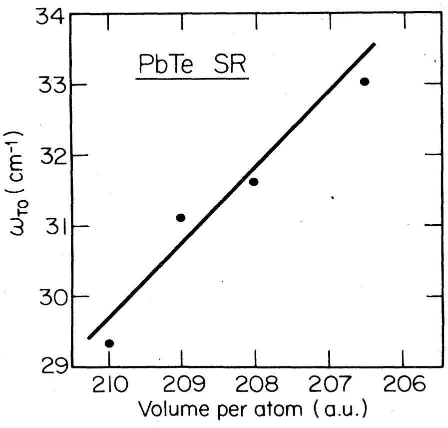

FIG. 15. $\omega_{\mathrm{TO}}(V)$ in cm^{-1} in PbTe. The range in V corresponds to a range in P from 0 to 8 kbar. The solid line is a good fit to the four calculated points. The calculation was done with 19 **k** points.

VII. SUMMARY AND CONCLUDING REMARKS

We have presented relativistic self-consistent pseudopotential calculations of the electronic structure and total energies of PbTe and SnTe in the rocksalt and rhombohedral structures. Specifically, we have calculated both band structures and fully-self-consistent *ab initio* charge densities. The latter were found to differ significantly from previous calculations. The structural properties calculated include equilibrium lattice parameters, bulk moduli, cohesive energies, phonon frequencies, and the shear elastic constant. Good agreement with experiment was obtained. In addition, we found $\omega_{\mathrm{TO}}(P)$ to be linear at small P, which is of interest in interpreting a recent experiment.

We discussed the sizes of numerical errors in Sec. II. An estimate of the accuracy to which the properties of the pseudocrystal reproduce those of the fully interacting electron-ion system is more difficult to obtain. The validity of the frozen core approximation and the transferability of the pseudopotentials can be estimated by comparing pseudoatom results with all-electron calculations for different atomic configurations. The accuracy of the LDA in approximating the true functional is also difficult to estimate. One hope is that, in calculating energy differences between similar structures, the errors cancel out to some degree. In the final analysis, the validity of the approximations and rough sizes of errors are judged by agreement with appropriate experimental quantities.

Finally, we note that we have found that for these materials, it is a valid approximation to neglect spin-orbit splitting in total-energy calculations resulting in a great savings in computational effort. This is important for the application of this technique to more complicated problems, e.g., pseudobinary alloys, defects such as vacancies and impurities, phonon calculations for $\mathbf{k}\neq 0$, and discussion of finite-temperature effects. The possibility of doing first-principles calculations on these materials should help in sorting out the variety of physical effects which determine their properties and thus in realizing their potential as simple systems for the study of structural transitions.

ACKNOWLEDGMENTS

This work was supported in part by National Science Foundation Grant No. DMR-83-02846. One of us (K.R.) would like to thank AT&T Bell Laboratories for support. We should also like to thank Dr. P. Littlewood, Professor S. McKnight, and Dr. D. DiVincenzo for helpful discussions.

[1] G. Nimtz and B. Schlicht, in *Narrow Gap Semiconductors,* Vol. 98 of *Springer Tracts in Modern Physics* (Springer, New York, 1983), and references therein.

[2] W. Jantsch, in *Dynamical Properties of IV-VI Compounds,* Vol. 99 of *Springer Tracts in Modern Physics* (Springer, New York, 1983), and references therein.

[3] A. Bussmann-Holder, H. Bilz, and P. Vogl, in *Dynamical Properties of IV-VI Compounds,* Vol. 99 of *Springer Tracts in Modern Physics* (Springer, New York, 1983), and references therein.

[4] M. E. Lines and A. M. Glass, *Principles and Applications of Ferroelectrics and Related Materials* (Clarendon, Oxford, 1977).

[5] N. J. Parada and G. W. Pratt, Jr., Phys. Rev. Lett. **22**, 180 (1969).

[6] S. Sugai, K. Murase, S. Katayama, S.Takaoka, S. Nishi, and H. Kawamura, Solid State Commun. **24**, 407 (1977).

[7] K. L. I. Kobayashi, Y. Kato, Y. Katayama, and K. F. Komatsubara, Phys. Rev. Lett. **37**, 772 (1976).

[8] L. Muldawer, J. Nonmetals **1**, 177 (1973).

[9] T. B. Zhukova and A. I. Zaslavskii, Kristallografiya **12**, 28 (1967) [Sov. Phys.—Crystallogr. **12**, 28 (1967)].

[10] M. Iizumi, Y. Hamaguchi, K. F. Komatsubara, and Y. Kato, J. Phys. Soc. Jpn. **38**, 443 (1975).

[11] H. A. Alperin, S. J. Pickart, J. J. Rhyne, and V. J. Minkiewicz, Phys. Lett. **40A**, 295 (1972).

[12] W. Cochran, R. A. Cowley, G. Dolling, and M. M. Elcombe, Proc. R. Soc. London **293**, 433 (1966).

[13] G. S. Pawley, W. Cochran, R. A. Cowley, and G. Dolling, Phys. Rev. Lett. **17**, 753 (1966).

[14] H. Burkhard, G. Bauer, and A. Lopez-Otero, Solid State Commun. **18**, 773 (1976).

[15] S. W. McKnight and M. K. El-Rayess, in *Proceedings of 17th International Conference on the Physics of Semiconductors, San Francisco* (Springer, New York, 1985), p. 1389.

[16] S. Sugai, K. Murase, and H. Kawamura, Solid State Commun. **23**, 127 (1977).

[17] T. Shimada, K. L. I. Kobayashi, Y. Katayama, and K. F. Komatsubara, Phys. Rev. Lett. **39**, 143 (1977).

[18] A. D. C. Grassie, J. A. Agapito, and P. Gonzalez, J. Phys. C **12**, L925 (1979).

[19] K. L. I. Kobayashi, Y. Kato, Y. Katayama, and K. F. Komatsubara, Solid State Commun. **17**, 875 (1975).

[20] I. Hatta and K. L. I. Kobayashi, Solid State Commun. **22**, 775 (1977).

[21] W. Cochran, Adv. Phys. **9**, 387 (1960).

[22] P. W. Anderson, in *Fizika Dielectrikov,* edited by G. I. Skanavi (Moscow, Akad. Nauk, 1960).

[23] G. Lucovsky and R. M. White, Phys. Rev. B **8**, 660 (1973).

[24] P. B. Littlewood, J. Phys. C **13**, 4855 (1980); **13**, 4875 (1980); in *Physics of Narrow Gap Semiconductors,* Vol. 152 of *Springer Lecture Notes in Physics* (Springer, New York, 1982), p. 238.

[25] W. Porod and P. Vogl, in *Physics of Narrow Gap Semiconductors,* Vol. 152 of *Lecture Notes in Physics* (Springer, New York, 1982), p. 247.

[26] G. Mula, in *Physics of Narrow Gap Semiconductors,* Vol. 152 of *Springer Lecture Notes in Physics* (Springer, New York, 1982), p. 252.

[27] See Ref. 3, Section 3.3.1.

[28] M. E. Lines, Phys. Rev. **177**, 797 (1969).

[29] H. Kawamura, in *Narrow Gap Semiconductors: Physics and Applications,* Vol. 133 of *Springer Lecture Notes in Physics,* edited by W. Zawasdki (Springer, New York, 1979), p. 470. See also, P. B. Littlewood, J. Phys. C **13**, 4875 (1980).

[30] H. Bilz, A. Bussman, G. Benedek, H. Buttner, and D. Strauch, Ferroelectrics **25**, 339 (1980).

[31] A. Bussmann-Holder, W. Kress, and H. Bilz, in *Physics of Narrow Gap Semiconductors,* Vol. 152 of *Springer Lecture Notes in Physics* (Springer, New York, 1982), p. 257.

[32] A. Zunger and M. L. Cohen, Phys. Rev. B **19**, 568 (1979).

[33] D. M. Bylander and L. Kleinman, Phys. Rev. B **27**, 3152 (1983); **29**, 1534 (1984).

[34] P. K. Lam and M. L. Cohen, Phys. Rev. B **24**, 4224 (1981); **25**, 6139 (1982).

[35] M. T. Yin and M. L. Cohen, Phys. Rev. B **26**, 3259 (1982); **26**, 5668 (1982).

[36] S. Froyen and M. L. Cohen, Solid State Commun. **43**, 447 (1982); Physica **117-118B&C** 561 (1983); Phys. Rev. B **28**, 3258 (1983).

[37] D. Vanderbilt and J. D. Joannopoulos, Solid State Commun. **35**, 535 (1980); Phys. Rev. B **27**, 6296 (1983).

[38] J. Ihm and J. D. Joannopoulos, Phys. Rev. Lett. **47**, 679 (1981).

[39] M. T. Yin and M. L. Cohen, Phys. Rev. B **24**, 6121 (1981).

[40] G. B. Bachelet, H. Greenside, G. A. Baraff, and M. Schlüter, Phys. Rev. B **24**, 4745 (1981).

[41] W. Andreoni, K. Maschke, and M. Schlüter, Phys. Rev. B **26**, 2314 (1982).

[42] S. Froyen and M. L. Cohen, Phys. Rev. B **29**, 3770 (1984).

[43] For a review of work up to 1982, see M. L. Cohen, Phys. Scr. **T1**, 5 (1982).

[44] M. T. Yin and M. L. Cohen, Phys. Rev. B **25**, 7403 (1982).

[45] D. Vanderbilt, Ph.D thesis, Massachusetts Institute of Technology, 1981.

[46] J. Ihm, A. Zunger, and M. L. Cohen, J. Phys. C **12**, 4409 (1979).

[47] G. B. Bachelet, D. R. Hamann, and M. Schlüter, Phys. Rev. B **26**, 4199 (1982).

[48] D. M. Ceperley, Phys. Rev. B **18**, 3126 (1978); D. M. Ceperley and B. J. Alder, Phys. Rev. Lett. **45**, 566 (1980); J. Perdew and A. Zunger, Phys. Rev. B **23**, 5048 (1981).

[49] P. O. Lowdin, J. Chem. Phys. **19**, 1396 (1951).

[50] H. J. Monkhorst and J. D. Pack, Phys. Rev. B **13**, 5188 (1976).

[51] L. Kleinman, Phys. Rev. B **21**, 2630 (1980).

[52] G. B. Bachelet and M. Schlüter, Phys. Rev. B **25**, 2103 (1982).

[53] M. Schlüter, G. Martinez, and M. L. Cohen, Phys. Rev. B **11**, 3808 (1975).

[54] B. Houston, R. E. Strakna, and H. S. Belson, J. App. Phys. **39**, 3913 (1968).

[55] D. R. Hamann, M. Schlüter, and C. Chiang, Phys. Rev. Lett. **43**, 1494 (1979).

[56] R. Hultgren *et al., Selected Values of the Thermodynamic Properties of the Elements* (American Society for Metals, Metals Park, Ohio, 1973).

[57] D. D. Wagman, Natl. Bur. Stand. Tech. Note **270-3**, 184 (1968); **270-3**, 191 (1968).

[58] R. F. Bis and J. R. Dixon, J. Appl. Phys. **40**, 1919 (1969).

[59] T. Seddon, S. C. Gupta, and G. A. Saunders, Solid State Commun. **20**, 69 (1976).

[60] A. G. Beattie, J. Appl. Phys. **40**, 4818 (1969).

[61] B. Houston and R. E. Strakna, Bull Amer. Phys. Soc. **9**, 646 (1964).

[62] G. Hausch, M. Gsanger, and E. Luscher, Z. Angew. Phys. **25**, 261 (1968).

[63] A. N. Mariano and K. L. Chopra, Appl. Phys. Lett. **10**, 282 (1967).

[64] R. Dalven, Infrared Phys. **9**, 141 (1969).